Data Processing Approaches on SPAD-Based d-TOF LiDAR Systems: A Review

Gongbo Chen, Christian Wiede, and Rainer Kokozinski

***Abstract*—With the rise of advanced driver assistance systems (ADAS), range sensors and their data processing methods are becoming more and more important. Light detection and ranging (LiDAR) sensors are attracting attention due to their unique advantages in terms of radial distance resolution and detection range. However, the study of LiDAR data processing is usually divorced from the LiDAR sensor measurement process itself. This leads to critical measurement information being overlooked. This paper seeks a breakthrough to improve the performance of single-photon-avalanche-diode-based direct time-of-flight LiDAR systems by reviewing the data processing stages and corresponding processing approaches for LiDAR measurements, starting from photon incidence and ending with high-level feature recognition. Firstly, we propose a LiDAR system model based on data generation and transfer. The data forms in such a LiDAR system are mainly classified into timestamps, time-correlated histograms, point cloud data, and high-level properties. Subsequently, data processing methods applied to each of these data forms are analyzed. A number of hardware solutions closely related to data transmission and control are also included in the discussion. The principles, limitations, and challenges of these methods are discussed in detail and the criteria for evaluation of time-correlated histograms in ADAS are proposed. Finally, the research gaps in data processing are summarized, and future directions for research development are presented.**

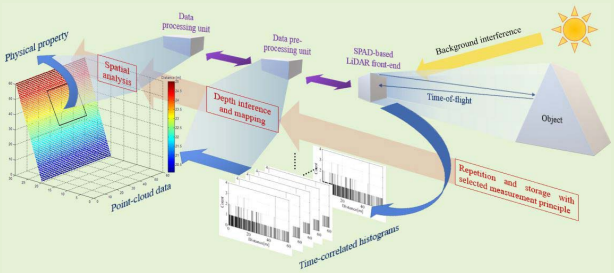

***Index Terms*— ADAS, data processing, LiDAR, point cloud, time of flight, time-correlated histograms.**

I. Introduction

TRAFFIC safety has always been a topic of great concern. In 2016, it is reported that 1,099,032 traffic accidents took place, resulting in 25,651 fatalities and more than 1.4 million injured people in Europe [1]. According to the report, accidents caused by distraction, drugs, alcohol, fatigue and over-speed driving, account for a large proportion. Mukhtar *et al*. discuss different types of distraction, fatigue, and immature driving behavior and point out that the human behavior is the main cause of accidents [2]. In order to reduce the safety hazards caused by human errors, advanced driver assistance systems (ADAS) is gaining traction as a solution to assist the driving behavior. Therein, depth information for environmental interaction is one of the most important sectors [3], which involves several range sensors and data processing technologies. The development of distance testing has lasted more than 20 years [4]. Common ranging technologies used in ADAS are radar, camera, ultrasonic, and light detection and ranging (LiDAR) [2]. An intuitive comparison among radar, camera and LiDAR is given in [5]. Since these ranging technologies have their own strengths and weaknesses, sensor fusion in automotive receives increasing interest to achieve performance beyond any single sensor technology. Among these technologies, LiDAR provides high range resolution and long depth range [5]–[7]. As applied in [8], the precise range information it provides will be indispensable for the safety in ADAS.

Since the first introduction of LiDAR technology, it has evolved into a number of different development branches, e.g. detectors, scanning mechanisms, and measuring modes. For the selection of the detector, a thorough comparison among avalanche photodiodes (APD), single photon avalanche diode (SPAD), and silicon photomultipliers is given in [9]. Depending on the sensor type, LiDAR technology can implement digital or analog readout. According to the scanning mechanism, LiDAR can be divided into flash, mechanical, MEMs, and optical phased arrays (OPA) [10]. According to the measuring mode, it can be categorized into direct time-of-flight (d-TOF) or indirect time-of-flight (i-TOF) mode. Basic principles of both modes are introduced and their advantages and

Manuscript received October 9, 2020; accepted November 1, 2020. Date of publication November 17, 2020; date of current version February 5, 2021. The associate editor coordinating the review of this article and approving it for publication was Dr. Marco J. Da Silva. *(Corresponding author: Gongbo Chen.)*

Gongbo Chen and Christian Wiede are with the Fraunhofer Institute of Microelectronic Circuits and Systems (IMS), 47057 Duisburg , Germany (e-mail: gongbo.chen@ims.fraunhofer.de).

Rainer Kokozinski is with the Department of Electronic Components and Circuits, University of Duisburg-Essen (UDE), 47057 Duisburg, Germany.

Digital Object Identifier 10.1109/JSEN.2020.3038487

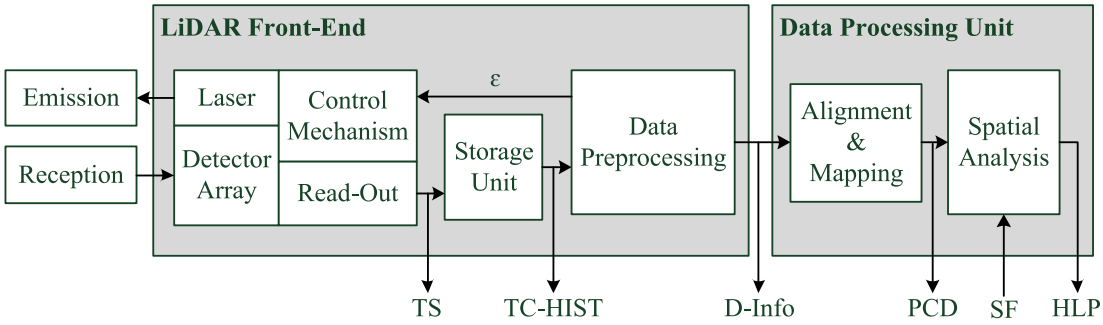

Fig. 1. LiDAR system structure for data transfer.

limitations are discussed in [3] and [11]. Modern outdoor LiDAR systems employ mostly d-TOF mode [10]. Although LiDAR technology have not been deployed in production automobiles to date [5], many LiDAR-based product prototypes are build both in the commercial sector [12]–[15] and for research uses [16]–[23]. Besides, several sensors are used for on-road testing and analysis as well. Waymo's fully self-driving technology, along with the LiDAR system developed by themselves, has driven over 20 million miles on real-world roads since 2009 [24]. Several LiDAR sensors are implemented and tested on road with different weather conditions in [25]. LiDAR's rich selection of components generate different data types. In addition to the hardware, research on LiDAR data processing is equally important. However, no research is found in reviewing the complete workflow of LiDAR data processing. In the following sections, we focus on SPAD-based d-TOF LiDAR systems and review different LiDAR data processing approaches.

The main contributions of this work are: 1) to provide an overview of the current state of development by sorting out existing approaches on the LiDAR data processing workflow, 2) to point out weaknesses or areas that have not been covered by research, 3) to discuss future research directions and advance the development of data processing.

Towards this end, the review is structured as follows: in section II, a data-transfer-based LiDAR system model is proposed. Then, the overall operating principles of the LiDAR system are presented and the terms used in this work are defined to facilitate the understanding of subsequent approaches. In section III, the existing data processing approaches in different stages of the processing workflow are discussed individually. A summary is provided, setting out the practical problems addressed by the existing approaches in tabular form. In section IV, the remaining problems and challenges are discussed. In section V, the final conclusion is given and an outlook is suggested.

II. System Structure and Measurement Process

One of the main goals of ADAS is to analyze the environmental information collected through sensors and ultimately obtain comprehensible high-level properties and decisions. To illustrate all stages of development in this process, a system structure is necessary. A generic architecture for simulation of ADAS sensors is proposed in [26]. Based on this, a LiDAR-specific system structure is introduced for object detection in [27]. However, the former focuses on commonality among multiple sensors for ADAS, while the latter places more emphasis on object detection by LiDAR sensors. Neither involve different stages in the LiDAR data processing. Therefore, we present a LiDAR system model based on data transfer in Fig. 1 in order to investigate the characteristics of different data forms and the hierarchy of corresponding analysis approaches.

As shown in Fig. 1, the LiDAR structure is divided into 2 parts: the LiDAR front-end and the data processing unit. The former includes hardware related units and the correlated embedded system for data pre-processing, while the latter focuses on stages of data processing. The overall working principle of such a LiDAR system can be categorized into the single photon round-trip measurement, the measurement accumulation and the data pre-processing, and the data main processing.

1) Single Photon Round-Trip Measurement: An active laser source is used in the LiDAR front-end, which emits laser pulses periodically. The time period between two consecutive pulses is referred as one measurement cycle. The detector array consists of multiple SPADs. SPAD is a special avalanche photon diode that is biased beyond the breakdown voltage. In this case, the avalanche effect can be triggered by a single photon and the diode will be broken down. Therefore, the SPADs theoretically has the ability to detect a single photon. This operating mode is often referred as Geiger mode [3], [28]. After the activation by a photon, the SPAD is insensitive for a period of time and loses its functionality and is unable to detect the next incident photons. This insensitive period is referred as dead time [29]. In practice, a quenching circuit is necessary for the SPADs to be able to detect a next photon after the breakdown in time. Firstly, the quenching circuit reduces the voltage and afterwards increase it again to the desired level by external circuits in order to reset the SPAD to the initial state. The signals ε are sent from the embedded system to control the operation of the laser, the quenching circuit and the readout.

The TOF will be calculated according to the laser round-trip time. After that, the TOF will be converted to a digital timestamp (TS) by a time-to-digital converter, which is the first accessible data in the LiDAR system, shown in Fig. 1. In the case of a fixed detection range, the digit number of the timestamp determine the distance resolution of the sensor.

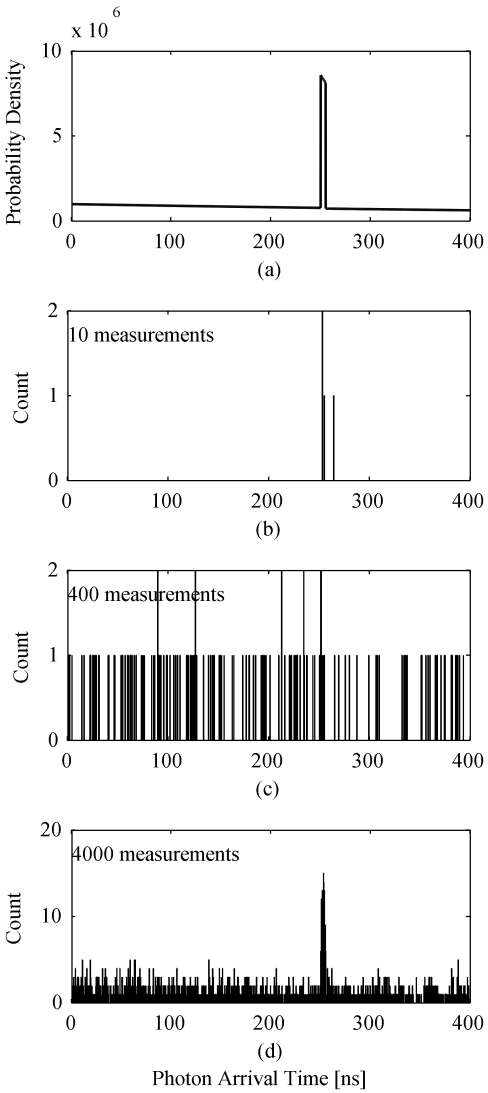

Fig. 2. Examples of TC-HISTs. a) is the ideal probability density function of the first arrived photon. b), c), and d) are simulated TC-HISTs with different number of measurements. Parameter settings are: background photon rate is 1MHz, received laser photon rate is 10 MHz, sensor resolution is 312.5 ps, laser pulse width is 5 ns, and TOF is 250 ns.

2) Measurement Accumulation and Data Pre-Processing: Although the SPAD has high sensitivity, it cannot distinguish between laser photons and ambient photons. Therefore, a single measurement is often unreliable. Time correlated single photon counting (TCSPC) technique [30], [31] is typically used to cope with this problem. It aggregates multiple consecutive TSs on a time-correlated histogram (TC-HIST). The time period of collecting and completing TC-HISTs from all SPADs is called a frame. In the flash LiDAR system, one frame is equal to the completion time for one TC-HIST. However, it is equal to the sum of completion time for all TC-HISTs in the scanning LiDAR system due to asynchrony. Therefore, the measurement number in a TC-HIST of the scanning LiDAR system is less than that of the flash LiDAR system in the same frame duration. Photon arrival times at a detector follows the Poisson process [32]. TCSPC processes can be divided into synchronized and asynchronized mode, which corresponds to the clock-driven architecture and event-driven architecture respectively [34]. Most TCSPC methods operate on the first photon counting mode, which follows the clock-driven architecture. An example of a clock-driven TC-HIST is shown in Fig. 2. In the TC-HIST, the y-axis represents the count number. The x-axis represents the time. TSs with the same value will accumulate on the same bin. The bin width on the x-axis can be equal or less than the TS resolution. As shown in Fig. 2, with the increasing number of collected TSs in a frame, the distance information and the noise floor become more and more intuitive. However, the required time to complete one frame increases as well.

A TC-HIST contains typically the noise feature, the sensor feature, the statistical feature, and the distance information (D-Info). After completing one frame, TC-HISTs are processed by certain algorithms on the embedded systems, e.g. peak detection, digital filters, and maximum likelihood estimation, aiming at acquiring D-Info. These algorithms will be introduced in Section III.

3) Data Main Processing: Finally, the set of all single-point D-Info inferred from TC-HISTs in one frame will form the point cloud data (PCD) by data alignment and mapping. Evidently, the PCD does not retain the information other than D-Info from the TC-HISTs. However, it contains information of the object spatial correlation [33]. Thus, by applying task-specific algorithms, high-level properties (HLP), e.g. object position, size, movement, and category, can be recovered from the PCD. Furthermore, our review shows that the PCD is the most commonly used LiDAR data in sensor fusion (SF) applications. However, the analyses on PCD are complex [33] and require powerful processing units, e.g. CPUs and GPUs.

III. Data Processing Methods on LiDAR Systems

In section III A - F, different data processing approaches are divided into six categories and explained focusing on their similarities in their working principles. Section III G included approaches with special uses or in the early research and development phase. In Section III H, the aforementioned approaches are summarized and discussed with the focus of their applications according to the applied data processing stages.

A. Optical Bandpass Filters

Due to the dead time, SPADs suffer from a saturation effect in the outdoor scenario [9]. Laser sources in LiDAR systems generate laser pulses in a specific wavelength, typically from 800 nm to 1550 nm [10], while the solar irradiance covers the full wavelength range. Therefore, optical bandpass filters can be used to remove irradiance at unwanted wavelengths [35]. In practical, the bandwidth cannot be smaller than 40 nm, due to the fluctuations in the laser wavelength produced by a Fabry-Perot laser source [36]. The use of more complex laser sources can further reduce the bandwidth, but will increase the product price. Nevertheless, since solar irradiance is highly significant in the wavelength range used in LiDAR systems [37], Süss *et al.* point out that the remaining ambient light can still saturate a SPAD, even when a 50 nm optical bandpass filter is used [38]. Therefore, additional methods must be carried out in order to reduce the probability of generating background-induced TSs.

B. Coincidence Counting

Coincidence counting, which originates in [39], is an effective measurement approach to further suppress the background

light. It involves several SPADs. These SPADs work in parallel. By predefining a coincidence level (CL), which consists of coincidence time interval t_c and a minimum photon number N_p, an output signal is generated only when more than N_p photons are detected during t_c. As long as no output signal is generated during the measurement cycle, the activated SPAD will be put back into operation after a short reboot time. This approach mitigates the saturation effect of SPADs and improves signal-to-background ratio [38]. LiDAR systems that use this method can operate normally in strong background light [11], [19], [40], [41]. Since this approach has a stronger inhibitory effect on triggering events below CL in comparison with the case of the triggering events above CL, the selection of a coincidence level is crucial. However, a proper CL strongly depends on ambient light intensity, received target light pulse intensity, target reflection, and target distance, which are always varying in practice. Beer *et al.* present an adaptive coincidence counting method, which enables the coincidence level adjustment in real-time [16].

Essentially, the approach uses pre-defined thresholds to reduce the overall generation rate of the output events. This means, it suppresses the false-triggering rate caused by the background light, as well as the triggering rate of the laser pulse. Therefore, the coincidence counting is effective when laser intensity is significantly higher than the background light intensity [38]. Otherwise, it yields little improvements and even deteriorates the measurement accuracy. Furthermore, SPADs in coincidence counting mode need to be triggered and rebooted more frequently than it is in the first photon counting mode. This results in some degree of statistical distortion e.g. missed counts and the after-pulsing effect. While shortening the rebooting time reduces the missed count rate, it exacerbates the after-pulsing effect [16]. Besides, the coincidence counting requires a set of SPADs implemented in a single pixel. This will lead to complex readout circuits and a sparse distribution of sensor measurement points in space.

C. Time-Gating

In a d-TOF LiDAR system, the emitted laser is a pulsed beam. The incident photon rate is the superposition of the laser pulse and background light during the arriving moment of the laser pulse $[t_1, t_2]$, and is equal to ambient photon rate in the rest of the time. In this case, the wanted signal is present only within $[t_1, t_2]$. This means the SPAD can only detect ambient photons during the most of the time, and therefore the effective triggering rate is low, when sufficient background light is present. In order to improve this situation, the time-gating technique is introduced [42]. The technique increases the effective detection rate by shortening the sensitive period of the SPAD. An example is shown in Fig. 2. In ideal case, by activating the SPADs right before the arrival moment, the risk of SPAD being triggered prematurely can be avoided. Kostamovaara *et al.* demonstrate the effectiveness of the technique in their experiment by applying different gate windows [36]. The technique can be implemented by combining SPAD's quenching circuits and gating schemes. The quenching circuits are responsible for the activation and rebooting of the SPADs [42]. Advanced SPAD imagers with gating features are designed and manufactured in [20], [41]. The gating scheme determines the practical application. For example, Apple Inc. designs a gating scheme to enable coarse and fine scanning to improve memory occupancy and measurement quality [43] .

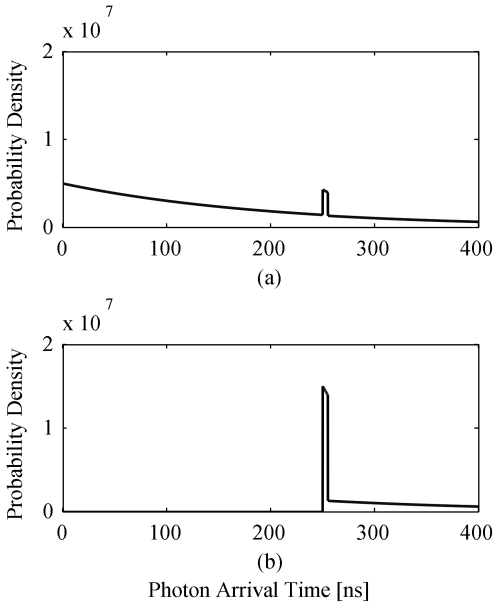

Fig. 3. Probability density function of first received photon. Parameter settings are: background photon rate is 5 MHz, received laser photon rate is 10 MHz, sensor resolution is 312.5 ps, laser pulse width is 5 ns, TOF is 250 ns. Activation moment of the SPAD: a) 0 ns, b) 250 ns.

Although the benefit of the time gating technique is significant, its limitation is quite obvious. A well-defined time period is inevitable if the technique is applied. However, it is very difficult to determine such a period. In [43], the effort of inferring a proper gating window is several times greater than that of inferring the exact D-Info.

D. Data Compression

Due to the high precision and wide range of LiDAR measurements, there are usually several thousands of bins in a TC-HIST. Considering that one measurement period is extremely short and that the detection array contains at least hundreds of SPADS, a LiDAR system can generate large amounts of data each second. An estimated data amount according to the size of the SPAD array and the sensor resolution is given in [44]. However, the data throughput and the storage capacity are restricted in ADAS. In order to transmit and process these data efficiently, data compression technology is necessary. Hornung *et al.* present Octomap, which is an open-source framework for three-dimensional mapping [45]. The framework is based on octrees and uses probabilistic occupancy estimation and synthesizes probabilistic representation, modeling of unmapped areas, and efficiency with respect to runtime and memory usage. Although it acts more as a mapping structure than a compression algorithm, it substantially improves memory efficiency. Golla *et al.* argue that the real-time performance of compression methods is necessary in many applications, e.g. robotics [46]. They introduce a real-time compression approach supporting incrementally acquired data and local decompression. The compression

approach is particularly remarkable in terms of its real-time performance. It can compress 1.5 million points per second.

In addition to the compression methods targeting the 3D PCD, the compression of data before the formation of the PCD is also of concern. A short review of low-level LiDAR data acquisition and compression can be found in [47]. Besides, histogram compression is another way to reduce data amount. Partial histogram readout is implemented in [21]. The approach includes several measurement stages. Measurements in the first stage starts with low range resolution and full detection range. Subsequently, a sub-detection-range is selected based on the result of the last stage, and the range resolution will increase. After several rounds of repetition, the method ultimately applies the maximum resolution only in a small sub-range. However, as reported, this method leads to reduced frame rate and noise tolerance.

E. Peak Detection and Digital Filters

In addition to filtering and optimizing the measurement data for the data generation, digital processing plays an important role in data denoising and data analysis as well.

Peak detection [21] is the simplest method obtaining distance information from TC-HISTs. By assuming the probability of receiving more than one photon within one measurement period is small enough to be negligible, i.e. under a low background photon rate, the background count follows the uniform distribution. The laser arrival moment can be easily caught by peak detection, during which the photon rate is the superposition of background photons and laser echo. However, peak detection only compares the count value in the individual bins and does not consider the effect of pulse waveform, resulting in low precision and robustness. Hence, the method requires a noise-free environment and a large number of measurement periods to obtain sufficient counts.

At the basis of peak detection, various of algorithms can be performed to improve TOF precision, such as Gaussian curve fitting and continuous wavelet transform [48]. In addition, digital filters are applied on TC-HISTs as well. For example, mean filter calculates the average of counts over the laser pulse width, allowing peak detection to be performed with sparse counts. Matched filter [49] maximizes the signal-to-noise ratio (SNR) of the laser pulse by weighting the count values individually. Center-of-mass filter [50] improves range precision by calculating the center-of-mass of the laser pulse. Since the background photon rate is relatively easy to obtain, the estimated noise floor is usually removed when the background light is significant. However, these filters need to process the complete TC-HIST and choose small sliding steps to ensure the precision. Therefore, they are demanding in terms of computational cost.

Kalman filter [51] is a recursive solution to the discrete-data linear filtering problem. Based on that, a non-linear version called extended Kalman filter is presented in [52]. In LiDAR systems, the Kalman filters are used for tracking and estimating the motion of identified objects e.g. lane prediction [53] [54].

F. Machine Learning

Machine learning (ML) is known as an empirical method, which can complete a specific task without programming the functions explicitly. In recent years, ML has been proved to be outperformed the classical methods with respect to the flexibility and capability in many fields [55]. One of the most important tasks of ML is inferring the interconnection of things by the observation of the presentative results, e.g. training samples. This coincides with the purpose of sensor data processing. Therefore, it receives increasing attention in sensor data processing areas, including LiDAR sensors. The design of a ML algorithm in ADAS follows the procedure of a pattern recognition system [56]: 1) data acquisition and pre-processing, 2) data representation, and 3) decision making. To this end, the encoder-decoder-based framework originated from machine translation [57], which modularizes the algorithm structure, becomes more and more predominant.

The objectives of ML algorithms are mainly twofold: 1) depth information optimization, e.g. depth-completion, calibration, and denoising. 2) HLP inference, e.g. object classification, allocation, and segmentation.

1) Depth Information Optimization: Due to the high radial resolution, the range information from LiDAR sensors is more precise than other range sensors. However, the LiDAR data are not noise-free, especially in the outdoor detection scenarios. Known problems include insufficient number of incoming photons due to low reflectivity, sparse spatial resolution, and large amounts of noise due to high background light intensity. These drawbacks can significantly degrade the performance of the post-processing [58].

Different approaches are proposed to cope with these problems. Altmann *et al*. proposes a new Bayesian reflectivity and depth models when the incoming photon flux is very low [59]. The model establishes Markovian dependencies according to the spatial correlations with neighboring pixels. Subsequently, an adaptive Markov chain Monte Carlo algorithm is applied to compute the Bayesian estimates of interest and perform Bayesian inference. In [60], an up-sampling method based on a convolutional neural network (CNN) is presented dealing with the limited spatial resolution of LiDAR data. Cheng *et al*. introduces a feedback loop to automatically clean the noise data in the PCD [58]. In addition, LiDAR data are used as a complement to range information in many sensor fusion applications. The most common example is the fusion between the LiDAR data and the stereo images [58], [61]–[63]. The use of images to guide the reconstruction of depth information is collectively known as depth completion. The so-called "depth images" generated from depth completion often inherit the resolution from stereo images and range information from LiDAR data.

2) High-Level Property Inference: Other approaches are aimed at deriving HLPs. Gargoum *et al*. divide possible features for pattern recognition in LiDAR data into on-road information, roadside information, and in conducting assessment of highway [64]. The property inference involved in ADAS can be categorized into 1) vehicle and pedestrian detection, 2) driver's state, behavior and identification, 3) traffic sign recognition, and 4) road detection and scene understand-

ing [65]. A machine vision based traffic sign detection methods are reviewed in [66].

Due to the powerful ability in image property inference [67], the CNN is the most applied method among all algorithms. Li *et al*. generates 3D bounding box from LiDAR data using a 2D fully convolutional network (FCN) [68]. In their further work, while retaining the original idea of the 2D FCN, a 3D FCN is proposed [69].

PointNet [70] is one of the pioneers on processing PCD based on the recursive neural network. Instead of transforming the PCD to 3D voxel grids or images, the method directly uses point data as inputs and outputs classification results or single-point based segmentation. Afterwards, PointNet++ [71] is presented as an upgraded version. It captures fine-granted patterns by applying the PointNet recursively on a nested partitioning of the input point set. Frustum PointNet [72] is the integrator of all PointNet versions, which takes RGB-D data as input for 3D object detection.

The complementarity between LiDAR data and stereo image has inspired researchers to investigate the joint solution on RGB-D data and has received satisfactory results [73]–[76]. In [75], the LiDAR front-view data is firstly up-sampled and then is aligned to the stereo image. A deep CNN is used to the reconfigured data. Instead of classical sliding windows [77] or the selective search [78], Zhao *et al*. employ LiDAR front-view data to generate region proposals [76]. The proposals are further mapped to the stereo image for the region of interest. This method achieves good results in terms of the inferring speed and accuracy. In addition to the stereo image and the LiDAR front-view data, the LiDAR bird-view data is used to apply additional features in [74]. Recent evidence shows that a simple network suffers from relative low accuracy [79] and the performance can be improved by adding additional layers [80]. However, it also makes the training challenging due to a large number of parameters and complex network structures. The residual network (ResNet) [81] is proposed to ease problems on a very deep neural network. Examples of applying ResNet on LiDAR data can be found in [61], [82]. Despite the network size, a modern machine learning algorithm considers generally only one specific task. Several tasks, such as plane estimation, inferring 3D bounding box, and object detection, are processed by individual algorithm blocks [73]. Through the concept of transfer learning [83], [84], the encoder-decoder network structure in [85], which shares an encoder while designs individual decoders for different tasks, can reduce the repetitive operations arising from simple combinations of algorithms. However, as reported in [58], even a small, five-layer network contains 25,000 parameters. Ren *et al*. argue that the real-time performance in autonomous driving is as important as the inference accuracy and proposed their SBNet to speed up the training and the calculation in CNN [82].

G. Further Approaches

BM3D is an image denoising strategy based on sparse 3-D transform-domain collaborative filtering [86]. The strategy first builds blocks by searching for proximity pixels with similar features, which is referred as grouping. After that, collaborative filtering by shrinkage in transform domain is applied to remove noise. Finally, the image is recovered by reverse transformation. The strategy is implemented on LiDAR data in [87].

Maximum likelihood estimation (MLE) is another method applied in imaging to determine the optimal parameters of the correlated model for the given data. In [50], the likelihood ratio test is used on the shape of the laser pulse. However, the experiment for the proposed approach is only carried out within 2 m. To the best of our knowledge, increasing the detection range can lead to an exorbitant computational cost. To simplify the computation of the MLE, an approximation, i.e. the log-matched filter [87], can be applied. However, for single pixel estimation, the efficiency of the MLE strongly depends on the SNR and data amount [88]. When the SNR is low or the data amount is small, the MLE gives inaccurate estimates. Kirmani *et al*. present a technique to obtain the single-pixel distance information based on the spatial correlations of neighboring pixels [89]. This work is extended in [87] and a better RMSE is reported in terms of depth recovery compared to the case using the BM3D and the log-matched filter.

The pile-up effect, which is an aberration existed in the SPAD-based system, is studied and the corresponding post-processing approach is proposed on the synchronized TCSPC process [90]. Besides, Rapp *et al*. focus their research on the asynchronized TCSPC process and proposes two Markov-chain-based methods for the histogram modelling and detector dead time compensation [91]. They demonstrate the positive effect of the presence of dead time as well.

H. Summary

In this section, the different approaches are divided into three categories in order to provide an overview of the state-of-the-art in different data processing stages:

1) Optimization Approaches for TC-HISTs: The first stage of data reception represents the process from photon incidence, triggering detector, to the generation of the triggering event. The approaches in this stage (shown in Table I) are mainly employed to mitigate the negative effects of background noise and hardware-induced data distortion. Since their working principles are closely related to the physical laws and hardware parameters, a new concept always requires a dedicated hardware implementation, resulting in a long research cycle. Nevertheless, the limitations of these methods make reliable measurements in outdoor scenarios still challenging. A holistic approach that combining hardware adjustment strategies and software processing algorithms may open up new possibilities.

2) Inference Approaches on TC-HISTs: The approaches applied in this stage (shown in Table II) are dedicated to inferring distance information in the TC-HIST. Converting the TC-HIST to the D-Info should be performed on embedded systems as much as possible to mitigate the data transmission overload. As a result, the performance of these methods is often limited by the resources available on the embedded system.

Unlike applications in odometry, LiDAR systems in ADAS typically requires a TC-HIST to be completed in a short period of time. This results in sparse counts in the TC-HIST.

TABLE I
OPTIMIZATION APPROACHES FOR TC-HISTS

Task	Approaches	Limitations
Background intensity suppression	Bandpass filter [35]	Fabrication and cost
	Time-gating [20], [41], [43]	Well-defined prior knowledge required
	Coincidence counting [11], [16], [19], [40], [41]	High intensity of laser echoes required
Compensation of hardware-induced distortion	Dead time compensation [91]	Asynchronized TCSPC only
	Pile-up compensation [90]	Large amount of counts required in a TC-HIST
Mitigation of transmission and storage overload	Low-Level data compression [47], compressive sampling [92]	Early stage of research on LiDAR data
	Partial histogram measurement strategy [21], [43]	Low frame rate Low background light tolerance

TABLE II
INFERENCE APPROACHES ON TC-HISTS

Task	Approach	Specification
Distance inference	Peak detection [21], [48]	Global maximum extraction
Precision improvement	Digital filters [49], [50]	Center-of-mass or Best SNR
	Maximum likelihood estimation [50]	Maximum likelihood probability

Direct use of the probability distribution of photon arrivals for distance prediction can result in large errors. Therefore, methods based on peak detection [21], [48], the best SNR [49], and center-of-mass [50] are proposed to obtain precise distance information. Maximum likelihood estimation and its approximation algorithm show effectiveness in inferring precise distance as well, but their large computational cost brings challenges to applications in ADAS [47].

3) Approaches on LiDAR Point Clouds: Approaches in this stage consider the PCD as raw data and do not involve features of measurement procedure and sensor front-ends. We divide the point-cloud-based approaches reviewed in this paper into five categories according to their tasks, shown in Table III. Except for PCD compression, other tasks exploit the rich spatial correlation of PCD. Therein, compare to the depth completion, approaches for denoising and correlation assumes that the PCD are defective and attempts to filter and restore the information on the sparse PCD. In contrast, depth completion considers the PCD to be noise-free and is more focused on inferring and complementing uncaptured pixels by the sparse PCD. The fusion of LiDAR and stereo image takes the advantage of their good complementarity, which guides LiDAR data to accomplish depth completion by the fine graphical information provided by the stereo image. The HLP extraction tasks in ADAS mainly include object detection

TABLE III
DATA PROCESSING APPROACHES ON PCD

Task	Input	Approaches
Mitigation of transmission and storage overload	LiDAR	OctoMap [45], real-time compression [46]
Denoising and correction	LiDAR	LWBA [59], BM3D [86], First-photon imaging [89]
Depth completion	LiDAR	NN+CNN [60]
	LiDAR + Image	LidarStereoNet [58], SSDL [61], Sparse-to-Dense [62], IGDU [63], GuideNet [93], NLSPN [94], UberATG-FuseNet [95], DeepLiDAR [96]
Object detection (pedestrian, cyclists and trucks)	LiDAR	PointNet [70], PointNet++ [71], 3D-FCN [69], SB-Net [82]
	LiDAR + Image	F-PointNet [72], F-ConvNet [97], Fusion-CNN [75] MODA [76], 3D-OPU [73], Multi-View 3D-ODN [74]
Road estimation	LiDAR	Kalman filters [53] [54], LoDNN [98], ChipNet [99]
	LiDAR + Image	PLARD [100], TVF-Net [101]

(pedestrian, cyclists and trucks) and road estimation, which are usually achieved through deep ML networks.

Due to the diversity of design concepts and implementations, a fair comparison between different approaches is difficult. To address this problem, the KITTI benchmark is proposed [102]. By using the same training dataset and the same evaluation criteria, up-to-date comparisons in depth completion, object detection, tracking and road detection can be found in [103]. It can be observed that a large portion of the leading algorithms utilize the LiDAR data in all tasks.

IV. DISCUSSIONS

Although the development of LiDAR technology is driving the evolution of ADAS, it still faces challenges from different sectors. In this section, we divide a LiDAR system into data pre-processing stage (the TC-HIST-based processing) and the main processing stage (the PCD-based processing) and discuss them separately.

A. Discussion on TC-HISTs

The data pre-processing outputs D-Info from individual pixels. In ADAS, the four important criteria used to measure the capability of the data pre-processing are memory occupancy, information update rate, measurement robustness and precision.

1) Memory Occupancy: The memory occupancy in a d-TOF LiDAR system does not depend on the number of measurements in a frame, but increases with detection range, range resolution, and field of view (FOV). State-of-the-art LiDAR systems have a relative long detection range, high range resolution, and wide FOV, thus placing a great deal of strain on data storage and transmission.

2) Information Update Rate: The information update rate decreases with the increase of measurements number per frame and information derivation time and data transfer volume. In applications, where real-time performance is not critical, the precision and robustness of LiDAR's measurement are superior. However, the timeliness in ADAS is salient. This makes long-time single-frame detections or distance inference meaningless. Therefore, the information update rate should be as high as possible in order to guarantee the real-time availability.

3) Measurement Robustness: LiDAR systems need to counteract both environment-induced and system-induced interference. The environment-induced interference in the outdoor scenario is complex, which mainly includes illumination conditions, object surface reflectance and weather. Among the system-induced disturbances, the SPAD dead time [29], the pile-up effect [90], and the after-pulsing effect [16] are of concern as well.

4) Measurement Precision: The hardware measurement precision depends on the resolution of the timer and the TDCs. The precision of distance inference depends on the hardware measurement precision, the performance of the applied algorithm, and the data quality in the TC-HIST. Therein, the data quality is the most important factor, which increases with the measurement number per frame. This results in a trade-off between the precision and the information update rate. The measurement precision is certainly one of the most important metrics. However, we argue that compared to the information update rate and the measurement robustness, the measurement precision is less critical. In a fast-changing environment, obtaining information within a defined margin of error in a short time is more valuable for timely decision making than striving for maximum precision. Therefore, a reasonable reduction in precision is desirable in order to improve information update rate and robustness.

A TC-HIST-based solution should focus on these four criteria. The optical bandpass filter [35] is a universal approach to improve the robustness against the ambient light. But that alone is not sufficient. Coincident counting [39] suppresses both ambient light and the echo, which makes it only suitable for strong illumination conditions and high echo intensity. However, due to the complex scenarios of surface reflectance and the angle of reflection, as well as eye-safety restrictions on the laser power [104], high echo intensity is difficult to guarantee. Recently proposed adaptive coincidence counting [16] can adjust the coincidence level to the illumination conditions, but still much relies on the echo intensity. By an appropriate gating scheme [43], the detection range can be reduced in a frame without sacrificing the total detection range of the system. In this way, the SPAD saturation due to the Poisson procedure is mitigated. Thus, both measurement robustness and precision can be improved and the memory occupancy can be reduced. However, using the gating scheme means that multiple frames are required for a single distance determination and thus results in a significant drop in the information update rate. Partial histogram readout [21] reduces the memory occupancy while reducing the robustness to the background illumination and information update rate.

The existing approaches for distance inference on the TC-HIST focuses themselves on improving precision while overlooking the robustness of the applied algorithms to interference. The reliability of these approaches is significantly reduced when the background light is strong or measurement number per frame is small. Therefore, it is necessary to develop an approach that focuses on robustness of the distance inference and information update rate.

B. Discussion on PCD

Most of the analysis approaches on PCD employ ML algorithms, especially the CNN with the encoder-decoder structure. They are computationally intensive and therefore require the support of powerful computational units. Currently, these algorithms are based on personal computers equipped with powerful CPUs and GPUs [103] and a mobile implementation on an embedded system remains challenging. Besides, the supervised ML approach is the most common variant. It requires large amount of correctly labeled training data with diversity. These data are difficult to obtain. The KITTI benchmark is one of the most popular datasets in this sector. However, there is a variety of LiDAR front-ends, the PCD they generate can vary widely among them in terms of sparsity, precision, and accuracy. Therefore, algorithms that have been proven effective on KITTI dataset alone may not be generalizable to other datasets. Researchers propose semi-supervised [61] or unsupervised [58] approaches to mitigate this problem. Besides, the development of the target simulators or complete virtual measurement environments can be an interesting topic.

In addition to using classical image processing networks after transforming PCD into images [69], [68], [82], researchers design various approaches to assist the distance inference and HLP recognition and report positive results, for example direct processing of point series [70]–[72], fusing PCD with images at different processing stages [58], [74]–[76], [93], [95], deriving ground normal as the intermediate information [73], [96], and inferring measurement confidence level [96] or neighbor-pixel dependence [59], [94]. In fact, some features, which are well-recorded in TC-HISTs, can be used to accelerate derivation. However, in previous researches, the main processing is loosely coupled to the pre-processing. On the one hand, most LiDAR front-ends discard useful information, such as the features of interference, sensor characteristics, and the confidence level of the measurement, in the process of converting TC-HISTs to the PCD. Only the distance information is inherited into PCD. On the other hand, the main processing considers the sensor front-end as a black-box [105] and does not concern the information before the PCD. The information loss leads to underutilization of LiDAR's measurement data.

Finally, the ultimate goal of analyzing data in ADAS is to aid decision making. Therefore, the relation between deep completion and HLP recognition (e.g. object detection and tracking) should be sequential. However, they seem to be parallel in the current study. On the one hand, the current benchmark for depth completion is the mean error. No study is found where the performance of HLP recognition is upgraded

by the data from depth completion approaches. On the other hand, the HLP recognition typically employs deep neural networks, but no study specifically indicated whether a part of the deep neural network performs the function of deep completion.

Although numerous works are carried out, there exists research gaps in the LiDAR data processing workflow. More research and development are needed to further improve the performance of LiDAR systems.

V. Conclusion & Outlook

In this paper, we firstly introduced a SPAD-based d-TOF LiDAR system model based on the data flow. Afterwards, data processing approaches in different stages presented in the model is reviewed. The evaluation criteria for the TC-HIST especially for ADAS are proposed and illustrated. Hence, we discussed the state-of-the-art and the challenges of LiDAR data analysis. Research gaps are summarized as follows:

1) LiDAR benchmark: the large number of configurable parameters makes the LiDAR front-end quite versatile. However, there is a lack of a widely accepted standard to evaluate and guide these variants uniformly.
2) Data analysis on TC-HIST: data analysis on TC-HISTs is unitary. Except measurement precision, sparse works are carried out in terms of memory occupancy, information update rate, and measurement robustness.
3) Holistic approaches on the LiDAR system: there are numerous point-cloud-based data optimization and high-level feature inference approaches. However, there exists information loss when converting low-level data to PCD. These approaches consider the sensor front-end is a black-box, few of them involve low-level data analysis to obtain useful information other than PCD.
4) Traceability and interpretability of ML approaches: the functionality of each part of the deep learning algorithm applied on LiDAR data remains unclear.
5) Generation of training data: large amount of correctly labeled training data with diversity is indispensable for the supervised ML approaches. However, these data are hard to obtain. Few works involve data acquisition methods with labeling or unsupervised ML approaches.
6) Excessive data amount: reducing data amount is imperative for a mobile implementation of LiDAR systems. Few works are carried out here. No data storage optimization method has been tested in outdoor scenarios and is reported to be lossless (or low-loss) in terms of data quality.

Therefore, we suggest that future works could be conducted in the following aspects:

1) Edge intelligence: TC-HISTs are distributed on the embedded systems and contain useful information other than depth and reflection. ML approaches can be applied on TC-HISTs associated with hardware adjustment strategy to increase the utilization of information and the system performance. For example, noise features and sensor characteristics can be learned by ML algorithms to improve the robustness of distance inference and inferring other potential properties. The inferred properties at this stage have good timeliness. Using these results as feedback may further improve the stability and reliability of measurements.
2) Investigation and analysis between data pre-processing and main processing: the key idea is enabling a seamless system by taking a holistic approach and maximizing the efficiency of the information exchange. On the one hand, the computational cost of deriving different low-level data features on the pre-processing stage can be investigated. The impact of low-level features on main processing in terms of system robustness, precision and information update rate can be compared. The groups of features with the highest overall benefit can be eventually implemented in one system. On the other hand, the results from the main processing can benefit the sensor front-end as well. For example, the high-level features can be used to guide the control signal generation of gating scheme and coincidence levels allowing the system to operate more efficiently and effectively.
3) Joint analysis between depth completion and high-level feature recognition: more research has to be carried out for the importance of the depth completion in ADAS by comparing the performance differences between algorithms that use depth completion data and those that directly take the original data.
4) Target simulator/virtual sensors and environment: direct road testing to collect measurement data with labels is inefficient and expensive. Research on a hardware-based target simulator can keep the testing within a laboratory. In this case, most of the environmental parameters are configurable, facilitating the construction of desired scenarios. In addition, by simulating target scenarios and virtual sensors, the entire testing process can take place in a virtual environment. The combination of simulated and real data will accelerate the development of data processing approaches.
5) Data compression: a variety of excellent compression algorithms exist in other application fields. The theoretical compatibility of these algorithms with LiDAR data can be analyzed and eventually evaluated on a LiDAR system in runtime.

The different research directions mentioned above will open up new possibilities for the development of LiDAR systems.

References

[1] *Annual Accident Report 2018*, Eur. Road Saf. Observatory, Brussels, Belgium, 2018. [Online]. Available: https://ec.europa.eu/info/about-european-commission/organisational-structure/locations_en#headquarters

[2] A. Mukhtar, L. Xia, and T. B. Tang, "Vehicle detection techniques for collision avoidance systems: A review," *IEEE Trans. Intell. Transp. Syst.*, vol. 16, no. 5, pp. 2318–2338, Oct. 2015, doi: 10.1109/TITS.2015.2409109.

[3] R. Horaud, M. Hansard, G. Evangelidis, and C. Ménier, "An overview of depth cameras and range scanners based on time-of-flight technologies," *Mach. Vis. Appl.*, vol. 27, no. 7, pp. 1005–1020, Oct. 2016, doi: 10.1007/s00138-016-0784-4.

[4] F. Blais, "Review of 20 years of range sensor development," *J. Electron. Imag.*, vol. 13, no. 1, pp. 231–240, Jan. 2004.

[5] S. Alland, W. Stark, M. Ali, and M. Hegde, "Interference in automotive radar systems: Characteristics, mitigation techniques, and current and future research," *IEEE Signal Process. Mag.*, vol. 36, no. 5, pp. 45–59, Sep. 2019, doi: 10.1109/MSP.2019.2908214.

[6] B. Behroozpour, P. A. M. Sandborn, M. C. Wu, and B. E. Boser, "Lidar system architectures and circuits," *IEEE Commun. Mag.*, vol. 55, no. 10, pp. 135–142, Oct. 2017, doi: 10.1109/MCOM.2017.1700030.

[7] M. Zaffar, S. Ehsan, R. Stolkin, and K. M. Maier, "Sensors, SLAM and long-term autonomy: A review," in *Proc. NASA/ESA Conf. Adapt. Hardw. Syst. (AHS)*, Aug. 2018, pp. 285–290.

[8] C. Premebida, G. Monteiro, U. Nunes, and P. Peixoto, "A lidar and vision-based approach for pedestrian and vehicle detection and tracking," in *Proc. IEEE Intell. Transp. Syst. Conf.*, Sep. 2007, pp. 1044–1049.

[9] K. Pasquinelli, R. Lussana, S. Tisa, F. Villa, and F. Zappa, "Single-photon detectors modeling and selection criteria for high-background LiDAR," *IEEE Sensors J.*, vol. 20, no. 13, pp. 7021–7032, Jul. 2020, doi: 10.1109/JSEN.2020.2977775.

[10] S. Royo and M. Ballesta-Garcia, "An overview of lidar imaging systems for autonomous vehicles," *Appl. Sci.*, vol. 9, no. 19, p. 4093, Sep. 2019, doi: 10.3390/app9194093.

[11] M. Perenzoni, D. Perenzoni, and D. Stoppa, "A 64×64-pixels digital silicon photomultiplier direct TOF sensor with 100-MPhotons/s/pixel background rejection and imaging/altimeter mode with 0.14% precision Up To 6 km for spacecraft navigation and landing," *IEEE J. Solid-State Circuits*, vol. 52, no. 1, pp. 151–160, Jan. 2017, doi: 10.1109/JSSC.2016.2623635.

[12] Velodyne LiDAR Inc. *Products Main Page*. Accessed: Jul. 2020. [Online]. Available: https://velodynelidar.com/

[13] *Ibeo Automotive Systems GmbH*. Accessed: Jul. 2020. [Online]. Available: https://www.ibeo-as.com/de/produkte

[14] *Quanergy Systems*. Accessed: Jul. 2020. [Online]. Available: https://quanergy.com/

[15] *Ouster*. Accessed: Jul. 2020. [Online]. Available: https://ouster.com/

[16] M. Beer, J. F. Haase, J. Ruskowski, and R. Kokozinski, "Background light rejection in SPAD-based LiDAR sensors by adaptive photon coincidence detection," *Sensors*, vol. 18, no. 12, p. 4338, 2018, doi: 10.3390/s18124338.

[17] D. Bronzi, Y. Zou, F. Villa, S. Tisa, A. Tosi, and F. Zappa, "Automotive three-dimensional vision through a single-photon counting SPAD camera," *IEEE Trans. Intell. Transp. Syst.*, vol. 17, no. 3, pp. 782–795, Mar. 2016, doi: 10.1109/TITS.2015.2482601.

[18] A. Martin *et al.*, "Photonic integrated circuit-based FMCW coherent LiDAR," *J. Lightw. Technol.*, vol. 36, no. 19, pp. 4640–4645, Oct. 1, 2018, doi: 10.1109/JLT.2018.2840223.

[19] C. Niclass, M. Soga, H. Matsubara, M. Ogawa, and M. Kagami, "A 0.18-μ m CMOS SoC for a 100-m-range 10-frame/s 200×96-pixel time-of-flight depth sensor," *IEEE J. Solid-State Circuits*, vol. 49, no. 1, pp. 315–330, Jan. 2014, doi: 10.1109/JSSC.2013.2284352.

[20] J. Nissinen, I. Nissinen, S. Jahromi, T. Talala, and J. Kostamovaara, "Time-gated CMOS SPAD and a quantum well laser diode with a CMOS driver for time-resolved diffuse optics imaging," in *Proc. IEEE Nordic Circuits Syst. Conf. (NORCAS): NORCHIP Int. Symp. Syst.–Chip (SoC)*, Piscataway, NJ, USA, Oct. 2018, pp. 1–4.

[21] C. Zhang, S. Lindner, I. M. Antolovic, J. Mata Pavia, M. Wolf, and E. Charbon, "A 30-frames/s, 252×144 SPAD flash LiDAR with 1728 dual-clock 48.8-ps TDCs, and pixel-wise integrated histogramming," *IEEE J. Solid-State Circuits*, vol. 54, no. 4, pp. 1137–1151, Apr. 2019, doi: 10.1109/JSSC.2018.2883720.

[22] G. Zhou, X. Zhou, J. Yang, Y. Tao, X. Nong, and O. Baysal, "Flash lidar sensor using fiber-coupled APDs," *IEEE Sensors J.*, vol. 15, no. 9, pp. 4758–4768, Sep. 2015, doi: 10.1109/JSEN.2015.2425414.

[23] A. Ingle, A. Velten, and M. Gupta, "High flux passive imaging with single-photon sensors," in *Proc. IEEE/CVF Conf. Comput. Vis. Pattern Recognit. (CVPR)*, Jun. 2019, pp. 6760–6769.

[24] *Waymo Main Page*. Accessed: Jul. 2020. [Online]. Available: https://waymo.com/tech/

[25] M. Jokela, P. Pyykonen, M. Kutila, and K. Kauvo, "LiDAR performance review in arctic conditions," in *Proc. IEEE 15th Int. Conf. Intell. Comput. Commun. Process. (ICCP)*, Sep. 2019, pp. 27–31.

[26] T. Hanke, N. Hirsenkorn, B. Dehlink, A. Rauch, R. Rasshofer, and E. Biebl, "Generic architecture for simulation of ADAS sensors," in *Proc. 16th Int. Radar Symp. (IRS)*, Jun. 2015, pp. 125–130.

[27] P. Rosenberger *et al.*, "Benchmarking and functional decomposition of automotive lidar sensor models," in *Proc. IEEE Intell. Vehicles Symp. (IV)*, Jun. 2019, pp. 632–639.

[28] B. F. Aull *et al.*, "Geiger-mode avalanche photodiodes for three-dimensional imaging," *Lincoln Lab. J.*, vol. 13, no. 2, pp. 335–350, 2002.

[29] S. Cova, M. Ghioni, A. Lacaita, C. Samori, and F. Zappa, "Avalanche photodiodes and quenching circuits for single-photon detection," *Appl. Opt.*, vol. 35, no. 12, pp. 1956–1976, 1996.

[30] D. V. O'Connor and D. Philips, *Time-Correlated Single Photon Counting*. London, U.K.: Academic, 1984.

[31] W. Becker, *Advanced Time-Correlated Single Photon Techniques* (Series in Chemical Physics). Berlin, Germany: Springer, 2005.

[32] D. L. Snyder and M. I. Miller, *Random Point Processes in Time and Space*. New York, NY, USA: Springer-Verlag, 1991.

[33] B. Schwarz, "Mapping the world in 3D," *Nature Photon.*, vol. 4, no. 7, pp. 429–430, Jul. 2010, doi: 10.1038/nphoton.2010.148.

[34] I. M. Antolovic, S. Burri, C. Bruschini, R. Hoebe, and E. Charbon, "Nonuniformity analysis of a 65-kpixel CMOS SPAD imager," *IEEE Trans. Electron Devices*, vol. 63, no. 1, pp. 57–64, Jan. 2016, doi: 10.1109/TED.2015.2458295.

[35] T. Fersch, R. Weigel, and A. Koelpin, Eds., "Challenges in miniaturized automotive long-range lidar system design," *Proc. SPIE*, vol. 10219, May 2017, Art. no. 102190T.

[36] J. Kostamovaara *et al.*, "On laser ranging based on high-Speed/Energy laser diode pulses and single-photon detection techniques," *IEEE Photon. J.*, vol. 7, no. 2, pp. 1–15, Apr. 2015, doi: 10.1109/JPHOT.2015.2402129.

[37] Rob Garner. *Solar Irradiance*. Accessed: Jul. 2020. [Online]. Available: https://www.nasa.gov/mission_pages/sdo/science/solar-irradiance.html

[38] A. Süss, V. Rochus, M. Rosmeulen, and X. Rottenberg, Eds., "Benchmarking time-of-flight based depth measurement techniques," SPIE OPTO, vol. 9751, Mar. 2016, Art. no. 975118.

[39] Walther Bothe. *Nobel Lecture–The Coincidence Method*. Accessed: Jul. 2020. [Online]. Available: https://www.nobelprize.org/prizes/physics/1954/bothe/lecture/

[40] M. M. Hayat, S. N. Torres, and L. M. Pedrotti, "Theory of photon coincidence statistics in photon-correlated beams," *Opt. Commun.*, vol. 169, nos. 1–6, pp. 275–287, Oct. 1999.

[41] D. Portaluppi, E. Conca, and F. Villa, "32×32 CMOS SPAD imager for gated imaging, photon timing, and photon coincidence," *IEEE J. Sel. Topics Quantum Electron.*, vol. 24, no. 2, pp. 1–6, Mar. 2018, doi: 10.1109/JSTQE.2017.2754587.

[42] A. Gallivanoni, I. Rech, and M. Ghioni, "Progress in quenching circuits for single photon avalanche diodes," *IEEE Trans. Nucl. Sci.*, pp. 3815–3826, Dec. 2010, doi: 10.1109/TNS.2010.2074213.

[43] A. K. Sharma, A. Laflaquière, G. A. Agranov, G. Rosenblum, and S. Mandai, "SPAD array with gated histogram construction," U.S. Patent 14 830 760, Feb. 23, 2017.

[44] I. Vornicu, A. Darie, R. Carmona-Galan, and A. Rodriguez-Vazquez, "Compact real-time inter-frame histogram builder for 15-bits high-speed ToF-imagers based on single-photon detection," *IEEE Sensors J.*, vol. 19, no. 6, pp. 2181–2190, Mar. 2019, doi: 10.1109/JSEN.2018.2885960.

[45] A. Hornung, K. M. Wurm, M. Bennewitz, C. Stachniss, and W. Burgard, "OctoMap: An efficient probabilistic 3D mapping framework based on octrees," *Auto. Robots*, vol. 34, no. 3, pp. 189–206, Apr. 2013, doi: 10.1007/s10514-012-9321-0.

[46] T. Golla and R. Klein, "Real-time point cloud compression," in *Proc. IEEE/RSJ Int. Conf. Intell. Robots Syst. (IROS)*, Sep. 2015.

[47] I. Maksymova, C. Steger, and N. Druml, "Review of LiDAR sensor data acquisition and compression for automotive applications," *Proceedings*, vol. 2, no. 13, p. 852, 2018, doi: 10.3390/proceedings2130852.

[48] K. Q. K. Nguyen, E. M. D. Fisher, A. J. Walton, and I. Underwood, "An experimentally verified model for estimating the distance resolution capability of direct time of flight 3D optical imaging systems," *Meas. Sci. Technol.*, vol. 24, no. 12, Dec. 2013, Art. no. 125001, doi: 10.1088/0957-0233/24/12/125001.

[49] G. Turin, "An introduction to matched filters," *IEEE Trans. Inf. Theory*, vol. 6, no. 3, pp. 311–329, Jun. 1960.

[50] S.-Y. Tsai, Y.-C. Chang, and T.-H. Sang, Eds., "SPAD LiDARs: Modeling and algorithms," in *Proc. 14th IEEE Int. Conf. Solid-State Integr. Circuit Technol. (ICSICT)*, vol. 3. Piscataway, NJ, USA, Oct./Nov. 2018, pp. 1–4. [Online]. Available: http://ieeexplore.ieee.org/servlet/opac?punumber=8540788

[51] R. E. Kalman, "A new approach to linear filtering and prediction problems," *J. Basic Eng.*, vol. 82, no. 1, pp. 35–45, Mar. 1960.

[52] S. J. Julier and J. K. Uhlmann, Eds., "A new extension of the Kalman filter to nonlinear systems," in *The Robotics Research Group*, Department of Engineering Science. Oxford, U.K.: Univ. Oxford, 1997.

[53] M. Thuy and F. León, "Lane detection and tracking based on lidar data," *Metrol. Meas. Syst.*, vol. 17, no. 3, pp. 311–321, Jan. 2010, doi: 10.2478/v10178-010-0027-3.

[54] G. Wang, J. Wu, R. He, and S. Yang, "A point cloud-based robust road curb detection and tracking method," *IEEE Access*, vol. 7, pp. 24611–24625, 2019, doi: 10.1109/ACCESS.2019.2898689.

[55] G. A. Fink, Ed., *Markov Models for Pattern Recognition: From Theory to Applications*. London, U.K.: Springer-Verlag, 2014.

[56] A. K. Jain, P. W. Duin, and J. Mao, "Statistical pattern recognition: A review," *IEEE Trans. Pattern Anal. Mach. Intell.*, vol. 22, no. 1, pp. 4–37, Jan. 2000, doi: 10.1109/34.824819.

[57] K. Cho, B. van Merrienboer, D. Bahdanau, and Y. Bengio, Eds., "On the properties of neural machine translation: Encoder–decoder approaches," in *Proc. 8th Workshop Syntax, Semantics Struct. Stat. Transl.*, Oct. 2014, pp. 103–111.

[58] X. Cheng, Y. Zhong, Y. Dai, P. Ji, and H. Li, "Noise-aware unsupervised deep lidar-stereo fusion," in *Proc. IEEE/CVF Conf. Comput. Vis. Pattern Recognit. (CVPR)*, Jun. 2019, pp. 6339–6348.

[59] Y. Altmann, X. Ren, A. McCarthy, G. S. Buller, and S. McLaughlin, "Lidar waveform-based analysis of depth images constructed using sparse single-photon data," *IEEE Trans. Image Process.*, vol. 25, no. 5, pp. 1935–1946, May 2016, doi: 10.1109/TIP.2016.2526784.

[60] J. Uhrig, N. Schneider, L. Schneider, U. Franke, T. Brox, and A. Geiger, "Sparsity invariant CNNs," in *Proc. Int. Conf. 3D Vision (3DV)*, Oct. 2017, pp. 11–20. [Online]. Available: https://arxiv.org/abs/1708.06500

[61] Y. Kuznietsov, J. Stuckler, and B. Leibe, "Semi-supervised deep learning for monocular depth map prediction," in *Proc. IEEE Conf. Comput. Vis. Pattern Recognit. (CVPR)*, Jul. 2017, pp. 6647–6655.

[62] F. Ma and S. Karaman, Eds., "Sparse-to-dense: Depth prediction from sparse depth samples and a single image," in *Proc. IEEE Int. Conf. Robot. Automat. (ICRA)*, May 2018.

[63] D. Ferstl, C. Reinbacher, R. Ranftl, M. Ruether, and H. Bischof, "Image guided depth upsampling using anisotropic total generalized variation," in *Proc. IEEE Int. Conf. Comput. Vis.*, Dec. 2013, pp. 993–1000.

[64] S. Gargoum and K. El-Basyouny, "Automated extraction of road features using LiDAR data: A review of LiDAR applications in transportation," in *Proc. 4th Int. Conf. Transp. Inf. Saf. (ICTIS)*, Aug. 2017, pp. 563–574.

[65] J. Borrego-Carazo, D. Castells-Rufas, E. Biempica, and J. Carrabina, "Resource-constrained machine learning for ADAS: A systematic review," *IEEE Access*, vol. 8, pp. 40573–40598, 2020, doi: 10.1109/ACCESS.2020.2976513.

[66] C. Liu, S. Li, F. Chang, and Y. Wang, "Machine vision based traffic sign detection methods: Review, analyses and perspectives," *IEEE Access*, vol. 7, pp. 86578–86596, 2019, doi: 10.1109/ACCESS.2019.2924947.

[67] A. Krizhevsky, I. Sutskever, and E. G. Hinton. *ImageNet Classification With Deep Convolutional Neural Networks*. Accessed: Jul. 2020. [Online]. Available: http://www.cs.toronto.edu/~hinton/absps/imagenet.pdf

[68] B. Li, T. Zhang, and T. Xia, "Vehicle detection from 3D lidar using fully convolutional network," 2016, *arXiv:1608.07916*. [Online]. Available: http://arxiv.org/abs/1608.07916

[69] B. Li, "3D fully convolutional network for vehicle detection in point cloud," in *Proc. IEEE/RSJ Int. Conf. Intell. Robots Syst. (IROS)*, Vancouver, BC, Canada Sep. 2017, pp. 1513–1518.

[70] R. Q. Charles, H. Su, M. Kaichun, and L. J. Guibas, "PointNet: Deep learning on point sets for 3D classification and segmentation," in *Proc. IEEE Conf. Comput. Vis. Pattern Recognit. (CVPR)*, Jul. 2017, pp. 652–660.

[71] C. R. Qi, L. Yi, H. Su, and L. J. Guibas, "PointNet++: Deep hierarchical feature learning on point sets in a metric space," 2017, *arXiv:1706.02413*. [Online]. Available: http://arxiv.org/abs/1706.02413

[72] C. R. Qi, W. Liu, C. Wu, H. Su, and L. J. Guibas, "Frustum pointnets for 3D object detection from RGB-D data," in *Proc. IEEE Conf. Comput. Vis. Pattern Recognit. (CVPR)*, Jun. 2018, pp. 918–927.

[73] X. Chen, K. Kundu, Y. Zhu, H. Ma, S. Fidler, and R. Urtasun, "3D object proposals using stereo imagery for accurate object class detection," *IEEE Trans. Pattern Anal. Mach. Intell.*, vol. 40, no. 5, pp. 1259–1272, May 2018, doi: 10.1109/TPAMI.2017.2706685.

[74] X. Chen, H. Ma, J. Wan, B. Li, and T. Xia, "Multi-view 3D object detection network for autonomous driving," in *Proc. IEEE Conf. Comput. Vis. Pattern Recognit. (CVPR)*, Jul. 2017, pp. 1907–1915.

[75] H. Gao, B. Cheng, J. Wang, K. Li, J. Zhao, and D. Li, "Object classification using CNN-based fusion of vision and LIDAR in autonomous vehicle environment," *IEEE Trans. Ind. Informat.*, vol. 14, no. 9, pp. 4224–4231, Sep. 2018, doi: 10.1109/TII.2018.2822828.

[76] X. Zhao, P. Sun, Z. Xu, H. Min, and H. Yu, "Fusion of 3D LIDAR and camera data for object detection in autonomous vehicle applications," *IEEE Sensors J.*, vol. 20, no. 9, pp. 4901–4913, May 2020, doi: 10.1109/JSEN.2020.2966034.

[77] P. Dollar, R. Appel, S. Belongie, and P. Perona, "Fast feature pyramids for object detection," *IEEE Trans. Pattern Anal. Mach. Intell.*, vol. 36, no. 8, pp. 1532–1545, Aug. 2014, doi: 10.1109/TPAMI.2014.2300479.

[78] J. R. R. Uijlings, K. E. A. van de Sande, T. Gevers, and A. W. M. Smeulders, "Selective search for object recognition," *Int. J. Comput. Vis.*, vol. 104, no. 2, pp. 154–171, Sep. 2013, doi: 10.1007/s11263-013-0620-5.

[79] W. Liu *et al.*, "SSD: Single shot MultiBox detector," in *Computer Vision—ECCV* (Lecture Notes in Computer Science), vol. 9905, B. Leibe, J. Matas, N. Sebe, and M. Welling, Eds. Cham, Switzerland: Springer, 2016, doi: 10.1007/978-3-319-46448-0_2.

[80] K. Simonyan and A. Zisserman, "Very deep convolutional networks for large-scale image recognition," 2014, *arXiv:1409.1556*. [Online]. Available: http://arxiv.org/abs/1409.1556

[81] K. He, X. Zhang, S. Ren, and J. Sun, "Deep residual learning for image recognition," in *Proc. IEEE Conf. Comput. Vis. Pattern Recognit. (CVPR)*, Jun. 2016, pp. 770–778.

[82] M. Ren, A. Pokrovsky, B. Yang, and R. Urtasun, "SBNet: Sparse blocks network for fast inference," in *Proc. IEEE/CVF Conf. Comput. Vis. Pattern Recognit.*, Jun. 2018, pp. 8711–8720.

[83] J. Donahue *et al.*, "DeCAF: A deep convolutional activation feature for generic visual recognition," 2013, *arXiv:1310.1531*. [Online]. Available: http://arxiv.org/abs/1310.1531

[84] J. Yosinski, J. Clune, Y. Bengio, and H. Lipson, "How transferable are features in deep neural networks?" in *Proc. 27th Adv. Neural Inf. Process. Syst.*, Dec. 2014, pp. 3320–3328. [Online]. Available: https://arxiv.org/abs/1411.1792

[85] M. Teichmann, M. Weber, M. Zöllner, R. Cipolla, and R. Urtasun, "Multinet: Real-time joint semantic reasoning for autonomous driving," in *Proc. IEEE Intell. Vehicles Symp. (IV)*, Jun. 2018, pp. 1013–1020.

[86] K. Dabov, A. Foi, V. Katkovnik, and K. Egiazarian, "Image denoising by sparse 3-D transform-domain collaborative filtering," *IEEE Trans. Image Process.*, vol. 16, no. 8, pp. 2080–2095, Aug. 2007, doi: 10.1109/tip.2007.901238.

[87] D. Shin, A. Kirmani, V. K. Goyal, and J. H. Shapiro, "Photon-efficient computational 3-D and reflectivity imaging with single-photon detectors," *IEEE Trans. Comput. Imag.*, vol. 1, no. 2, pp. 112–125, Jun. 2015, doi: 10.1109/TCI.2015.2453093.

[88] S. M. Key. *Fundamentals Of Statistical Signal Processing–Estimation Theory*. Accessed: Jul. 2020. [Online]. Available: http://users.isr.ist.utl.pt/~pjcro/temp/Fundamentals%20Of%311-32120Statistical%20Signal%20Processing–Estimation%20Theory-Kay.pdf

[89] A. Kirmani *et al.*, "First-photon imaging," *Science*, vol. 343, no. 6166, pp. 58–61, Jan. 2014, doi: 10.1126/science.1246775.

[90] A. K. Pediredla, A. C. Sankaranarayanan, M. Buttafava, A. Tosi, and A. Veeraraghavan, "Signal processing based pile-up compensation for gated single-photon avalanche diodes," Jun. 2018. [Online]. Available: https://arxiv.org/abs/1806.07437

[91] J. Rapp, Y. Ma, R. M. A. Dawson, and V. K. Goyal, "Dead time compensation for high-flux ranging," *IEEE Trans. Signal Process.*, vol. 67, no. 13, pp. 3471–3486, Jul. 2019, doi: 10.1109/TSP.2019.2914891.

[92] E. J. Candes and M. B. Wakin, "An introduction to compressive sampling," *IEEE Signal Process. Mag.*, vol. 25, no. 2, pp. 21–30, Mar. 2008, doi: 10.1109/MSP.2007.914731.

[93] J. Tang, F.-P. Tian, W. Feng, J. Li, and P. Tan, "Learning guided convolutional network for depth completion," *IEEE Trans. Image Process.*, Aug. 2019. [Online]. Available: https://arxiv.org/abs/1908.01238

[94] J. Park, K. Joo, Z. Hu, C.-K. Liu, and I. So Kweon, "Non-local spatial propagation network for depth completion," 2020, *arXiv:2007.10042*. [Online]. Available: http://arxiv.org/abs/2007.10042

[95] Y. Chen, B. Yang, M. Liang, and R. Urtasun, "Learning joint 2D-3D representations for depth completion," in *Proc. IEEE/CVF Int. Conf. Comput. Vis. (ICCV)*, Oct. 2019, pp. 10023–10032.

[96] J. Qiu *et al.*, "DeepLiDAR: Deep surface normal guided depth prediction for outdoor scene from sparse LiDAR data and single color image," in *Proc. IEEE/CVF Conf. Comput. Vis. Pattern Recognit. (CVPR)*, Jun. 2018, pp. 3313–3322.

[97] Z. Wang and K. Jia, "Frustum ConvNet: Sliding frustums to aggregate local point-wise features for amodal 3D object detection," 2019, *arXiv:1903.01864*. [Online]. Available: http://arxiv.org/abs/1903.01864

[98] L. Caltagirone, S. Scheidegger, L. Svensson, and M. Wahde, "Fast LIDAR-based road detection using fully convolutional neural networks," in *Proc. IEEE Intell. Vehicles Symp. (IV)*, Jun. 2017, pp. 1019–1024.

[99] Y. Lyu, L. Bai, and X. Huang, "ChipNet: Real-time LiDAR processing for drivable region segmentation on an FPGA," *IEEE Trans. Circuits Syst. I, Reg. Papers*, vol. 66, no. 5, pp. 1769–1779, May 2019, doi: 10.1109/TCSI.2018.2881162.

[100] Z. Chen, J. Zhang, and D. Tao, "Progressive LiDAR adaptation for road detection," *IEEE/CAA J. Automatica Sinica*, vol. 6, no. 3, pp. 693–702, May 2019, doi: 10.1109/JAS.2019.1911459.
[101] S. Gu, Y. Zhang, J. Yang, J. M. Alvarez, and H. Kong, "Two-view fusion based convolutional neural network for urban road detection," in *Proc. IEEE/RSJ Int. Conf. Intell. Robots Syst. (IROS)*, Nov. 2019, pp. 6144–6149.
[102] A. Geiger, P. Lenz, and R. Urtasun, Eds., "Are we ready for autonomous driving? The kitti vision benchmark suite," in *Proc. IEEE Conf. Comput. Vis. Pattern Recognit.*, Jun. 2012, pp. 3354–3361.
[103] *Karsruhe Institute of Technology and Toyota Technological Institute*. The KITTI Vison Benchmark Suite. Accessed: Aug. 2020. [Online]. Available: http://www.cvlibs.net/datasets/kitti/index.php
[104] *Safety of Laser Products—Part 1: Equipment Classification*, IEC, document 60825-1, May 2014. [Online]. Available: https://www.vde-verlag.de/iec-normen/220821/iec-60825-1-2014.html
[105] M. D. Adams, "Lidar design, use, and calibration concepts for correct environmental detection," *IEEE Trans. Robot. Autom.*, vol. 16, no. 6, pp. 753–761, Dec. 2000, doi: 10.1109/70.897786.

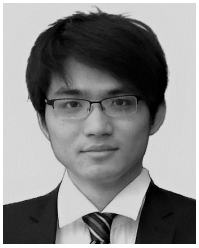

Gongbo Chen was born in Fujiang, China. He received the B.Eng. degree in electrical engineering from the China University of Mining and Technology, China, in 2016, and the M.Sc. degree in embedded systems engineering from the University of Duisburg-Essen, Duisburg, Germany, in 2018. He is currently pursuing the Ph.D. degree in electrical engineering with the Department of Embedded Artificial Intelligence, Fraunhofer Institute for Microelectronic Circuits and Systems, Duisburg.

His research interests include light detection and ranging systems, sensor data processing, and artificial intelligence on embedded systems.

Christian Wiede received the B.Sc. and M.Sc. degrees in biomedical engineering from the Ilmenau University of Technology, Ilmenau, Germany, in 2011 and 2013, respectively, and the Ph.D. degree in electrical engineering and information technology from the Chemnitz University of Technology, Chemnitz, Germany, in 2018.

He is specialized in the field of computer vision, machine learning, artificial intelligence, and embedded systems. He is currently working with Fraunhofer IMS, as the Head of Embedded AI.

Rainer Kokozinski was born in Oberhausen, Germany. He received the Dipl.-Ing. degree in electrical engineering and the Dr.-Ing. degree from the University of Duisburg, Duisburg, Germany, in 1990 and 1996, respectively.

In 1990, he joined the Signal Processing and System Design Department, Fraunhofer Institute of Microelectronic Circuits and Systems, Duisburg, working in the area of analog and mixed analog-digital CMOS and BiCMOS IC design. Among other things he was involved in design of microelectronic circuits and systems, RF circuits, A/D- and D/A-converters, switched capacitor circuits, and image sensors. From 1998 to 1999, he was with Toshiba Electronics Europe, Düsseldorf, Germany, where he headed the development of high-speed CMOS interface cells as well as the development of mixed-signal telecommunication ICs, e.g., for xDSL applications. He is currently a Professor with the University Duisburg-Essen, Duisburg, and the Head of Research Coordination with the Fraunhofer Institute of Microelectronic Circuits and Systems. His research interests include design of microelectronic circuits and systems, analog and digital signal processing as well as design techniques for medical implants, artificial intelligence, functional safety, harsh environments, and optical sensors.